

Article

# **CH<sub>3</sub>NH<sub>3</sub>Cl Assisted Solvent Engineering for Highly Crystallized and Large Grain Size Mixed-Composition (FAPbI<sub>3</sub>)<sub>0.85</sub>(MAPbBr<sub>3</sub>)<sub>0.15</sub> Perovskites**

Yihui Li <sup>1</sup>, Taiyang Zhang <sup>1</sup>, Feng Xu <sup>1</sup>, Yong Wang <sup>1</sup>, Ge Li <sup>1</sup>, Yang Yang <sup>2,\*</sup> and Yixin Zhao <sup>1,\*</sup>

<sup>1</sup> School of Environmental Science and Engineering, Shanghai Jiao Tong University, Shanghai 200240, China; yihuiliwv@sjtu.edu.cn (Y.L.); sun.zhang1988@gmail.com (T.Z.); 1934380351@sjtu.edu.cn (F.X.); wyong9512@163.com (Y.W.); 5111619052@sjtu.edu.cn (G.L.)

<sup>2</sup> Clean Energy Research Institute, China Huaneng Group, Beijing 102209, China

\* Correspondence: yangyang@qny.chng.com.cn (Y.Y.); yixin.zhao@sjtu.edu.cn (Y.Z.)

Academic Editor: Wei Zhang

Received: 17 July 2017; Accepted: 2 September 2017; Published: 5 September 2017

**Abstract:** High-quality mixed-cation lead mixed-halide (FAPbI<sub>3</sub>)<sub>0.85</sub>(MAPbBr<sub>3</sub>)<sub>0.15</sub> perovskite films have been prepared using CH<sub>3</sub>NH<sub>3</sub>Cl additives via the solvent engineering method. The UV/Vis result shows that the addition of additives leads to enhanced absorptions. XRD and SEM characterizations suggest that compact, pinhole-free and uniform films can be obtained. This is attributable to the crystallization improvement caused by the CH<sub>3</sub>NH<sub>3</sub>Cl additives. The power conversion efficiency (PCE) of the F-doped SnO<sub>2</sub> (FTO)/compact-TiO<sub>2</sub>/perovskite/Spiro-OMeTAD/Ag device increases from 15.3% to 16.8% with the help of CH<sub>3</sub>NH<sub>3</sub>Cl additive.

**Keywords:** perovskite; mixed-cation; mixed-halide; additive; CH<sub>3</sub>NH<sub>3</sub>Cl; solvent engineering

---

## 1. Introduction

Organic-inorganic hybrid lead halide perovskites have many attractive features such as tunable band gaps, easy-to-make properties, high optical absorption coefficients and superior charge transport properties. Therefore, they have become one of the most promising materials for optoelectronic applications, and the perovskite solar cells have reached a certified power conversion efficiency (PCE) of 22.1% [1–13]. The typical 3D hybrid lead halide perovskite has the classical APbX<sub>3</sub> structure, and the tunable composition for A and X components offers perovskites sufficient freedom in tuning structures and properties [1,3,14–20]. In particular, mixed-cation and mixed-halide perovskites have been an effective approach to optimize the properties of lead halide perovskites [5,21]. For example, the (FAPbI<sub>3</sub>)<sub>0.85</sub>(MAPbBr<sub>3</sub>)<sub>0.15</sub> perovskite is a popular recipe used for solar cells with enhanced performance and stabilities [5]. In spite of the advancement, it is still a challenging task to simultaneously control the film morphology and crystalline quality. It is thus urgent to explore a method to gain high-quality films and improve perovskite crystallization. In previous studies on the MAPbI<sub>3</sub> perovskite, the additive method was an effective way to control perovskite crystallization and growth in simple solution chemistry [22–35]. In general, additives can be divided into several types: Organic molecules [25,27–29,36,37], inorganic or ammonium salts [23,30–35], polymers [26] and ionic liquids [22]. Different additives may have different functional mechanisms. For example, the additive can provide homogenous nucleation sites to improve uniformity. It can also coordinate with metal ions to decrease the crystallization rate and enlarge crystals [38–40], and highly efficient semitransparent perovskite solar cells can be achieved [41,42]. In addition, it can change the surface energy to control the crystal growth direction. However, the impact of additives on the mixed composition perovskite is still an area awaiting more explorations.

In this work, we deposit the mixed-cation and mixed-halide  $(\text{FAPbI}_3)_{0.85}(\text{MAPbBr}_3)_{0.15}$  perovskite using  $\text{CH}_3\text{NH}_3\text{Cl}$  (MACl) additives. Our results indicate that the MACl additive has little impact on the optical properties of the  $(\text{FAPbI}_3)_{0.85}(\text{MAPbBr}_3)_{0.15}$  perovskite film but can significantly increase crystallinity and crystal grain size.

## 2. Results and Discussion

These  $(\text{FAPbI}_3)_{0.85}(\text{MAPbBr}_3)_{0.15}$  precursor films with or without MACl additives all turned orange after anti-solvent treatments without thermal annealing (0, 0.15, 0.3 molar ratio MACl with perovskite precursor solution donated as 0 MACl, 0.15 MACl and 0.3 MACl, respectively). The XRD patterns of these stable films before annealing are listed in Figure 1a. Firstly, a typical characteristic peak of perovskite appeared in all these precursor films. Meanwhile, an unknown peak located at  $\sim 12^\circ$  existed in all these precursor films, which might be ascribed to an intermediate phase owing to the complex between the solvent and the perovskite precursor. Interestingly, the peak intensity of this unknown intermediate decreased with the increase of the molar ratio of MACl. The intermediate peak in the precursor film using 0.3 MACl additives became much weaker while the perovskite peak was stronger than in the precursor film without MACl. This indicates that MACl can affect or accelerate the formation of the perovskite phase and inhibit the intermediate phase in these un-annealed films. This indexed intermediate phase is highly likely to be a complex of Pb, I, MA, solvent. The UV/Vis spectra are listed in Figure 1b. All these precursor films showed a characteristic peak at around 510–520 nm without obvious absorption at longer wavelengths although there were some perovskite phases found in these precursor films.

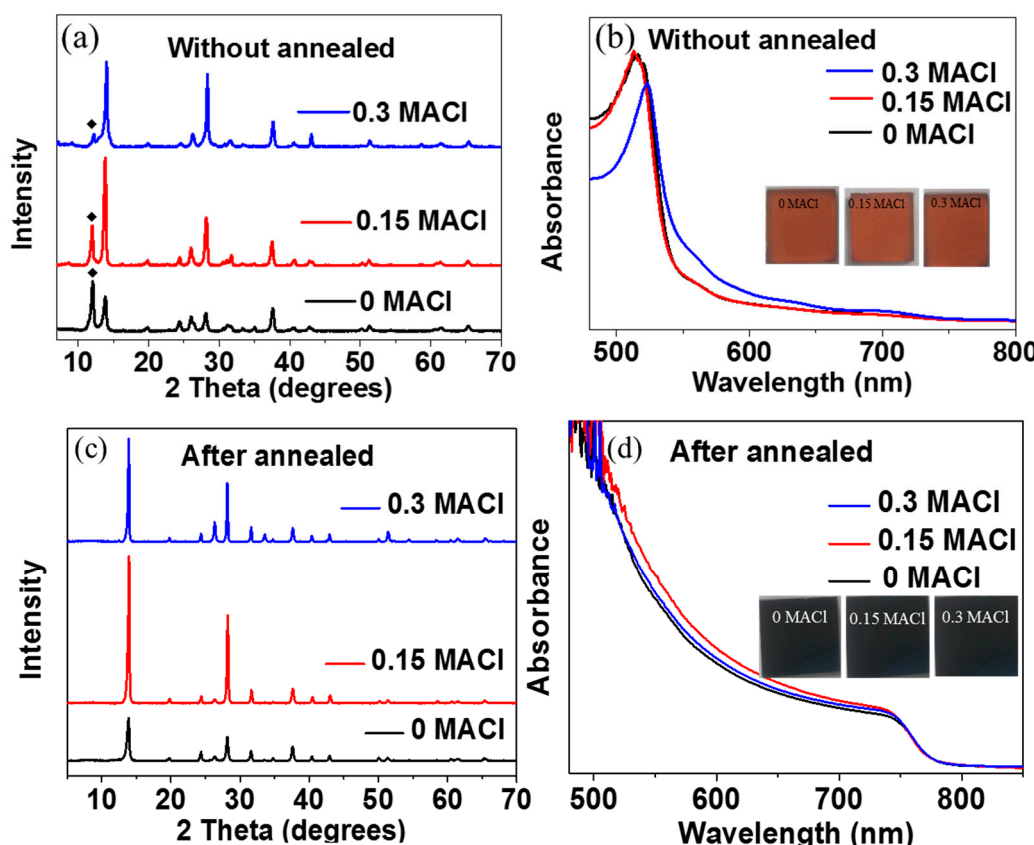


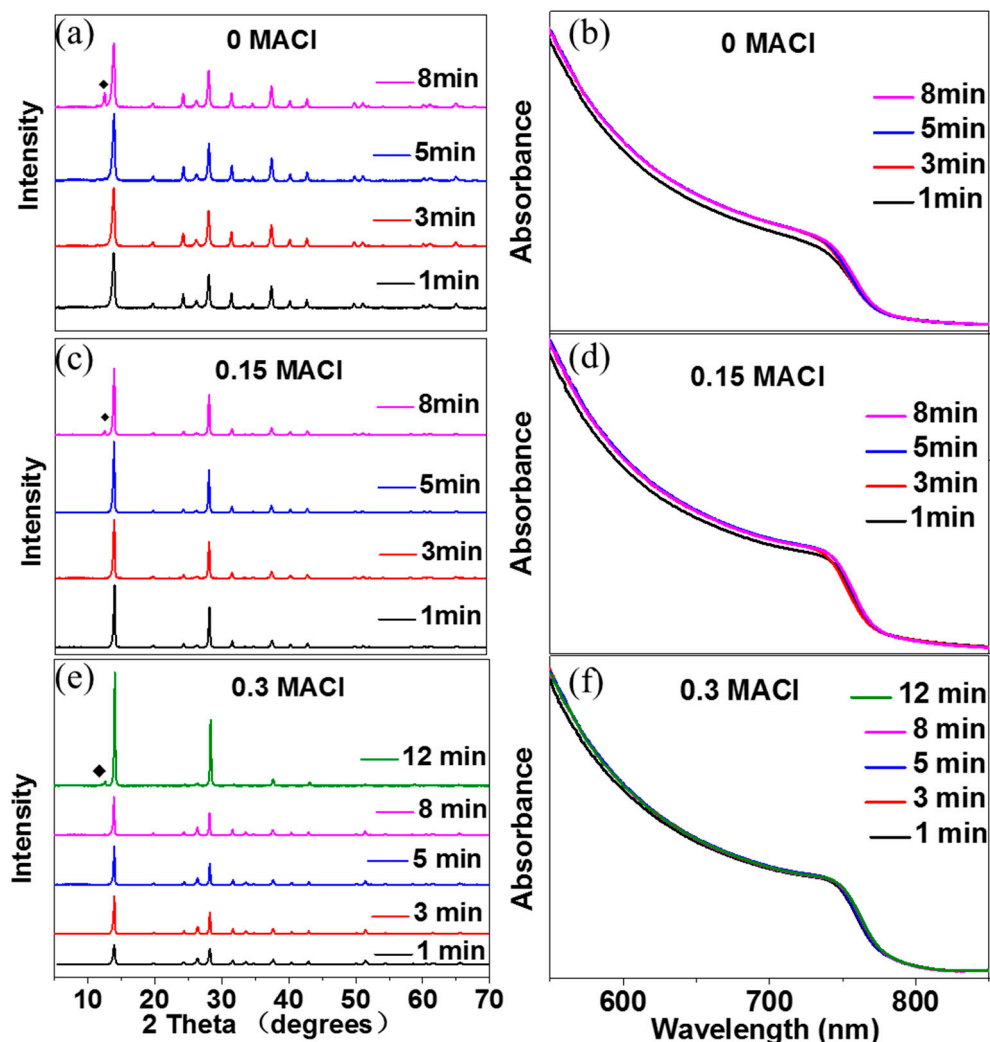
**Figure 1.** (a) The XRD patterns and (b) UV/Vis spectra of  $(\text{FAPbI}_3)_{0.85}(\text{MAPbBr}_3)_{0.15}$  films using 0, 0.15 and 0.3 MACl additives (a,b) without having been annealed and (c,d) after having been annealed. Insert: Precursor film images. ♦: the peak of the intermediate.

In order to investigate the film change before and after annealing, the XRD patterns and UV/Vis spectra of  $(\text{FAPbI}_3)_{0.85}(\text{MAPbBr}_3)_{0.15}$  on FTO glasses containing different amounts of MACl are listed in Figure 1c,d. All the orange precursor films turned dark after thermal annealing (see the insert images). The XRD patterns showed that the intermediate peak in all the precursor films disappeared and the samples with MACl additives had the same characteristic peaks of  $(\text{FAPbI}_3)_{0.85}(\text{MAPbBr}_3)_{0.15}$  perovskites as the sample without MACl [43]. The UV/Vis spectra of these samples were almost the same, which is consistent with the XRD patterns. Although these  $(\text{FAPbI}_3)_{0.85}(\text{MAPbBr}_3)_{0.15}$  samples were similar in the phase purity and UV/Vis absorption, the diffraction intensity was considerably enhanced in samples with the MACl additive, especially in the 0.15 MACl sample as shown in Figure 1c. This indicates that the MACl additive can significantly enhance the crystallinity of  $(\text{FAPbI}_3)_{0.85}(\text{MAPbBr}_3)_{0.15}$ . The XRD and UV/Vis spectra indicated that MACl greatly improved the perovskite crystallization, especially in the 0.15 MACl sample. It is worth noting that there was no Cl EDX signal found in these annealed 0.15 MACl and 0.3 MACl perovskite films. This means that MACl only functions as a “crystallization improver” affecting the crystal growth process and can be totally removed after annealing.

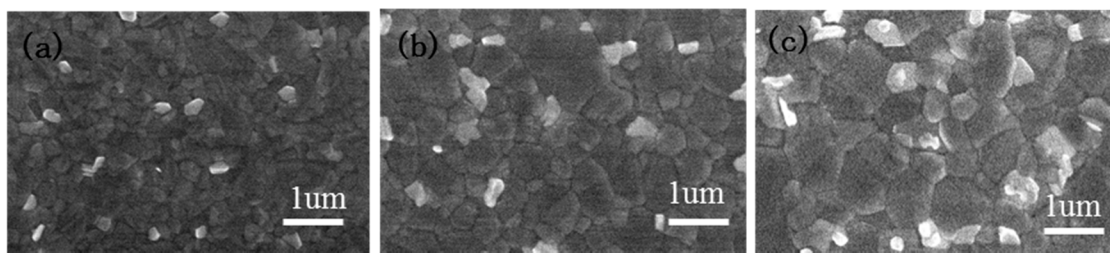
In order to further understand the perovskite crystallization process with and without MACl, we have investigated these perovskite films annealed for different times. Figure 2 lists the XRD patterns and UV/Vis spectrum evolution of the  $(\text{FAPbI}_3)_{0.85}(\text{MAPbBr}_3)_{0.15}$  perovskite films prepared from 0, 0.15 and 0.3 MACl with different annealing times. The annealing temperature was 150 °C and different annealing times have been tested: 1 min, 3 min, 5 min, 8 min and 12 min (for 0.3 MACl). The above paragraph has suggested that the crystallinity of the perovskite grown from precursors with MACl was better than the corresponding one without MACl. Based on the XRD and UV/Vis spectra results in Figure 2a,b, the crystallization process of the perovskite without MACl additives was that the solvent evaporated and the perovskite crystallization finished in the first 3 min. The perovskite film then exhibited the highest absorbance and XRD intensities. During the period of 5–8 min, the loss of MAI or MABr started to happen in the perovskite without MACl additives. The over-annealing exceeding 5 min then resulted in the appearance of PbI<sub>2</sub>. Over-annealing is usually adopted to obtain the PbI<sub>2</sub> passivation effect. According to the XRD patterns and UV/Vis evolution of the perovskites with 0.15 MACl and 0.3 MACl additives, it seems that MACl can retard the crystallization of the  $(\text{FAPbI}_3)_{0.85}(\text{MAPbBr}_3)_{0.15}$  perovskite, although MACl can also help to reduce the intermediate phase in the precursor films. As shown in Figure 2c–f, the 0.15 MACl and 0.3 MACl samples also exhibited the standard  $(\text{FAPbI}_3)_{0.85}(\text{MAPbBr}_3)_{0.15}$  perovskite XRD peaks and reached the maximal absorbance after 1–3 min annealing. However, their XRD intensities kept growing (especially for the 0.3 MACl sample), which might account for the enhanced crystallinity as observed in Figure 1. These MACl additives could also prevent the release of MAI since MACl needed to be expelled before MAI. However, PbI<sub>2</sub> was also observed in both the 0.15 MACl and 0 MACl samples after annealing for 8 min (Figure 2a,c), and PbI<sub>2</sub> appeared at 12 min in the 0.3 MACl sample (Figure 2e). The crystallinity of PbI<sub>2</sub> in the sample without MACl was higher than the one with MACl. Consequently, a weaker PbI<sub>2</sub> XRD peak was found in the 0.15 MACl and 0.3 MACl samples.

From the above-mentioned discussion, the MACl additive can significantly affect the crystallization of the  $(\text{FAPbI}_3)_{0.85}(\text{MAPbBr}_3)_{0.15}$  perovskite. The SEM was taken to further understand the effect of additives on their crystallinity or grain sizes. Figure 3a,c show the SEM images of  $(\text{FAPbI}_3)_{0.85}(\text{MAPbBr}_3)_{0.15}$  perovskite films prepared from 0 MACl, 0.15 MACl and 0.3 MACl. The perovskite crystal sizes in the 0 MACl sample are ~200–300 nm, which is typical for the regular solvent engineering process. Besides the  $(\text{FAPbI}_3)_{0.85}(\text{MAPbBr}_3)_{0.15}$  perovskite crystals, there were also some bright spots and they were probably the PbI<sub>2</sub> residues, which were all formed at the grains size similar to the previous report. With the MACl additive, the  $(\text{FAPbI}_3)_{0.85}(\text{MAPbBr}_3)_{0.15}$  perovskites showed larger crystal grain sizes. The crystal size of the 0.15 MACl sample increased to ~400 nm and that of the 0.3 MACl sample further increased to ~500 nm. They both had some PbI<sub>2</sub> residues existing at the grain boundary. Interestingly, the 0.3 MACl sample seemed to have more PbI<sub>2</sub> residues than

the 0.15 MACl sample and also the 0 MACl one. Usually, the large crystal grain can reduce charge recombination and promotes charge transport.



**Figure 2.** XRD patterns and UV/Vis spectra of  $(\text{FAPbI}_3)_{0.85}(\text{MAPbBr}_3)_{0.15}$  films with (a,b) 0, (c,d) 0.15 and (e,f) 0.3 MACl annealed for 1 min, 3 min, 5 min and 8 min at  $150\text{ }^\circ\text{C}$ .  $\blacklozenge$ :  $\text{PbI}_2$ .



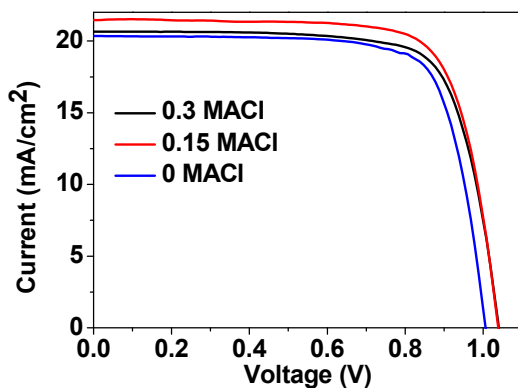
**Figure 3.** SEM images of  $(\text{FAPbI}_3)_{0.85}(\text{MAPbBr}_3)_{0.15}$  perovskite films using (a) 0, (b) 0.15 and (c) 0.3 MACl additives at  $150\text{ }^\circ\text{C}$ .

Table 1 lists the photovoltaic parameters of these  $(\text{FAPbI}_3)_{0.85}(\text{MAPbBr}_3)_{0.15}$  perovskite solar cells based on the planar device configuration of FTO/c-TiO<sub>2</sub>/perovskite/Spiro-OMeTAD/Ag. The 0.15 MACl device exhibited improved photovoltaic performance with increased  $J_{\text{sc}}$ ,  $V_{\text{oc}}$  and

Fill Factor (FF) compared to the 0 MACl device. The efficiency of the 0.3 MACl device was higher than that of the 0 MACl device but lower than that of the 0.15 MACl device. Figure 4 shows the typical J-V curves of these  $(\text{FAPbI}_3)_{0.85}(\text{MAPbBr}_3)_{0.15}$  perovskite solar cells using different molar ratios of MACl additives.

**Table 1.** Photovoltaic parameters of the FTO/c-TiO<sub>2</sub>/Perovskite/Spiro-OMeTAD/Ag devices with various molar ratios of MACl additives.

Samples	$J_{sc}$ (mA/cm <sup>2</sup> )	$V_{oc}$ (V)	FF (%)	PCE (%)
0.3 MACl	$20.6 \pm 0.32$	$1.04 \pm 0.01$	$74 \pm 2$	$15.9 \pm 0.4$
0.15 MACl	$21.3 \pm 0.45$	$1.04 \pm 0.01$	$76 \pm 2$	$16.8 \pm 0.3$
0 MACl	$20.2 \pm 0.76$	$1.01 \pm 0.02$	$75 \pm 4$	$15.3 \pm 0.7$



**Figure 4.** The typical J-V curves of the perovskite solar cells based on  $(\text{FAPbI}_3)_{0.85}(\text{MAPbBr}_3)_{0.15}$  using different molar ratios of MACl additives.

### 3. Conclusions

In summary, we have developed a MACl-assisted solvent engineering method to deposit the  $(\text{FAPbI}_3)_{0.85}(\text{MAPbBr}_3)_{0.15}$  perovskite film. The MACl additive can impact the crystallization process of the perovskite, which can be used as an additive for improving the thin-film quality of efficient semitransparent perovskite solar cells. The MACl additive can accelerate the crystallization of the precursor film to the perovskite phase but retard the crystallization of the perovskite phase during the thermal annealing process. Consequently, the MACl additive with a suitable MACl content (0.15 MACl) contributes to the formation of homogeneous and large grain perovskite films. The average PCE of the FTO/c-TiO<sub>2</sub>/perovskite/Spiro-OMeTAD/Ag device increases from 15.3% to 16.8% after utilizing the 0.15 MACl additive. The additive assisted solvent engineering method would be a promising strategy to optimize the deposition of high-quality perovskite films.

### 4. Materials and Methods

**Materials:** Patterned FTO glasses were etched with metallic Zn and HCl aqueous solution (2M) and then cleaned. A 20 nm thick compact TiO<sub>2</sub> layer deposited on the patterned FTO substrate was prepared by spray pyrolysis of 0.2 M Ti(IV) bis(ethyl acetoacetate)-diisopropoxide in 1-butanol solution at 450 °C, followed by annealing at 450 °C for one hour. MACl was synthesized by reacting methylamine (33 wt % ethanol solution) and 33 wt % hydrochloride acid with the molar ratio of 1.2:1 in an ice bath for 2 h with stirring, followed by vacuum drying and cleaning with acetonitrile. PbI<sub>2</sub>, PbBr<sub>2</sub>, CH<sub>3</sub>NH<sub>3</sub>Br(MABr), N,N-Dimethylformamide (DMF), dimethyl sulfoxide (DMSO) and chlorobenzene were purchased from Sigma-Aldrich and FAI was purchased from Shanghai MaterWin New Materials Co., Ltd.

**Device preparation:** The 1M  $(\text{FAPbI}_3)_{0.85}(\text{MAPbBr}_3)_{0.15}$  perovskite was prepared by mixing stoichiometric FAI,  $\text{PbI}_2$ , MABr and  $\text{PbBr}_2$  with the 0.85:0.85:0.15:0.15 molar ratio in DMF/DMSO (4/1 v/v). MACl molar ratios of 0, 0.15, 0.3 were added to the precursor solution, respectively. An amount of 80  $\mu\text{L}$  of the perovskite solution was spread on the substrate and spin coated in a two-step program at 1000 and 4000 rpm for 10 and 30 s, respectively. During the second step, 250  $\mu\text{L}$  of chlorobenzene was used as an anti-solvent and dripped on the top of the film 15 s prior to the end of the program. The substrates were then annealed at 150 °C in a glovebox. The hole transport layer was deposited on top of the perovskite film at 4000 rpm for 30 s using the hole transport material (HTM) solution, which consisted of 0.1 M spiro-MeOTAD, 0.035 M bis (trifluoromethane) sulfonamide lithium salt (Li-TFSi), and 0.12 M 4-tert-butylpyridine (tBP) in chlorobenzene/acetonitrile (10:1, v/v) solution. Finally, a 150-nm thick Ag film was deposited as a counter electrode using thermal evaporation.

**Characterization:** The photocurrent-voltage ( $J$ - $V$ ) characteristic of perovskite solar cells was measured with a 2401 source meter (Keithley, Cleveland, OH, USA) at a scan rate of 0.05 V/s under simulated AM1.5G illumination using Enlitech's 3A light source (Newport Corp., Irvine, CA, USA). The X-ray diffraction (XRD) measurement of perovskite films was performed using an X-ray diffractometer (Rigaku D/Max 2200, Rigaku Corporation, Tokyo, Japan) with Cu Ka radiation. Absorption spectra were measured using a UV/Vis spectrometer (Cary-6000i, Agilent Technologies, Santa Clara, CA, USA). The morphologies of perovskite films were characterized on a FEI Sirion 200 (Hillsboro, OR, USA) scanning electron microscope (SEM).

**Acknowledgments:** Yixin Zhao acknowledges the support of the NSFC (Grants 51372151 and 21303103) and Houyingdong Grant (151046).

**Author Contributions:** Yixin Zhao and Yang Yang conceived, designed the experiments and wrote the manuscript; Yihui Li performed the experiments and wrote the paper; Feng Xu and Taiyang Zhang performed the experiments and analyzed the data.

**Conflicts of Interest:** The authors declare no conflict of interest.

## References

- Stranks, S.D.; Eperon, G.E.; Grancini, G.; Menelaou, C.; Alcocer, M.J.; Leijtens, T.; Herz, L.M.; Petrozzi, A.; Snaith, H.J. Electron-hole diffusion lengths exceeding 1 micrometer in an organometal trihalide perovskite absorber. *Science* **2013**, *342*, 341–344. [[CrossRef](#)] [[PubMed](#)]
- Nie, W.; Tsai, H.; Asadpour, R.; Blanc, J.C.; Neukirch, A.J.; Gupta, G.; Crochet, J.J.; Chhowalla, M.; Tretiak, S.; Alam, M.A.; et al. High-efficiency solution-processed perovskite solar cells with millimeter-scale grains. *Science* **2015**, *347*, 522–525. [[CrossRef](#)] [[PubMed](#)]
- Noh, J.H.; Im, S.H.; Heo, J.H.; Mandal, T.N.; Seok, S.I. Chemical management for colorful, efficient, and stable inorganic-organic hybrid nanostructured solar cells. *Nano Lett.* **2013**, *13*, 1764–1769. [[CrossRef](#)] [[PubMed](#)]
- Im, J.-H.; Lee, C.-R.; Lee, J.-W.; Park, S.-W.; Park, N.-G. 6.5% efficient perovskite quantum-dot-sensitized solar cell. *Nanoscale* **2011**, *3*, 4088–4093. [[CrossRef](#)] [[PubMed](#)]
- Jeon, N.J.; Noh, J.H.; Yang, W.S.; Kim, Y.C.; Ryu, S.; Seo, J.; Seok, S.I. Compositional engineering of perovskite materials for high-performance solar cells. *Nature* **2015**, *517*, 476–480. [[CrossRef](#)] [[PubMed](#)]
- Liu, M.; Johnston, M.B.; Snaith, H.J. Efficient planar heterojunction perovskite solar cells by vapour deposition. *Nature* **2013**, *501*, 395–398. [[CrossRef](#)] [[PubMed](#)]
- Zhao, L.C.; Luo, D.Y.; Wu, J.; Hu, Q.; Zhang, W.; Chen, K.; Liu, T.H.; Liu, Y.; Zhang, Y.F.; Liu, F.; et al. High-performance inverted planar heterojunction perovskite solar cells based on lead acetate precursor with efficiency exceeding 18%. *Adv. Funct. Mater.* **2016**, *26*, 3508–3514. [[CrossRef](#)]
- Kim, H.S.; Lee, C.R.; Im, J.H.; Lee, K.B.; Moehl, T.; Marchioro, A.; Moon, S.J.; Humphry-Baker, R.; Yum, J.H.; Moser, J.E.; et al. Lead iodide perovskite sensitized all-solid-state submicron thin film mesoscopic solar cell with efficiency exceeding 9%. *Sci. Rep.* **2012**, *2*, 591. [[CrossRef](#)] [[PubMed](#)]
- Kojima, A.; Teshima, K.; Shirai, Y.; Miyasaka, T. Organometal halide perovskites as visible-light sensitizers for photovoltaic cells. *J. Am. Chem. Soc.* **2009**, *131*, 6050–6051. [[CrossRef](#)] [[PubMed](#)]

10. Burschka, J.; Pellet, N.; Moon, S.J.; Humphry-Baker, R.; Gao, P.; Nazeeruddin, M.K.; Gratzel, M. Sequential deposition as a route to high-performance perovskite-sensitized solar cells. *Nature* **2013**, *499*, 316–319. [[CrossRef](#)] [[PubMed](#)]
11. Yang, M.; Zhang, T.; Schulz, P.; Li, Z.; Li, G.; Kim, D.H.; Guo, N.; Berry, J.J.; Zhu, K.; Zhao, Y. Facile fabrication of large-grain  $\text{CH}_3\text{NH}_3\text{PbI}_{3-x}\text{Br}_x$  films for high-efficiency solar cells via  $\text{CH}_3\text{NH}_3\text{Br}$ -selective ostwald ripening. *Nat. Commun.* **2016**, *7*, 12305. [[CrossRef](#)] [[PubMed](#)]
12. Zhao, Y.; Zhu, K. Organic-inorganic hybrid lead halide perovskites for optoelectronic and electronic applications. *Chem. Soc. Rev.* **2016**, *45*, 655–689. [[CrossRef](#)] [[PubMed](#)]
13. Yin, W.J.; Shi, T.; Yan, Y. Unique properties of halide perovskites as possible origins of the superior solar cell performance. *Adv. Mater.* **2014**, *26*, 4653–4658. [[CrossRef](#)] [[PubMed](#)]
14. Parrott, E.S.; Milot, R.L.; Stergiopoulos, T.; Snaith, H.J.; Johnston, M.B.; Herz, L.M. Effect of structural phase transition on charge-carrier lifetimes and defects in  $\text{CH}_3\text{NH}_3\text{SnI}_3$  perovskite. *J. Phys. Chem. Lett.* **2016**, *7*, 1321–1326. [[CrossRef](#)] [[PubMed](#)]
15. Chen, Y.; Li, B.; Huang, W.; Gao, D.; Liang, Z. Efficient and reproducible  $\text{CH}_3\text{NH}_3\text{PbI}_{3-x}(\text{SCN})_x$  perovskite based planar solar cells. *Chem. Commun.* **2015**, *51*, 11997–11999. [[CrossRef](#)] [[PubMed](#)]
16. Tai, Q.; You, P.; Sang, H.; Liu, Z.; Hu, C.; Chan, H.L.; Yan, F. Efficient and stable perovskite solar cells prepared in ambient air irrespective of the humidity. *Nat. Commun.* **2016**, *7*, 11105. [[CrossRef](#)] [[PubMed](#)]
17. Zhou, Y.; Yang, M.; Pang, S.; Zhu, K.; Padture, N.P. Exceptional morphology-preserving evolution of formamidinium lead triiodide perovskite thin films via organic-cation displacement. *J. Am. Chem. Soc.* **2016**, *138*, 5535–5538. [[CrossRef](#)] [[PubMed](#)]
18. Wang, Z.K.; Li, M.; Yang, Y.G.; Hu, Y.; Ma, H.; Gao, X.Y.; Liao, L.S. High efficiency Pb-In binary metal perovskite solar cells. *Adv. Mater.* **2016**, *28*, 6695–6703. [[CrossRef](#)] [[PubMed](#)]
19. Saliba, M.; Matsui, T.; Domanski, K.; Seo, J.Y.; Ummadisingu, A.; Zakeeruddin, S.M.; Correa-Baena, J.P.; Tress, W.R.; Abate, A.; Hagfeldt, A.; et al. Incorporation of rubidium cations into perovskite solar cells improves photovoltaic performance. *Science* **2016**, *354*, 206–209. [[CrossRef](#)] [[PubMed](#)]
20. Nie, Z.; Yin, J.; Zhou, H.; Chai, N.; Chen, B.; Zhang, Y.; Qu, K.; Shen, G.; Ma, H.; Li, Y.; et al. Layered and pb-free organic-inorganic perovskite materials for ultraviolet photoresponse: (010)-Oriented  $(\text{CH}_3\text{NH}_3)_2\text{MnCl}_4$  thin film. *ACS Appl. Mater. Interfaces* **2016**, *8*, 28187–28193. [[CrossRef](#)] [[PubMed](#)]
21. Xu, F.; Zhang, T.; Li, G.; Zhao, Y. Mixed cation hybrid lead halide perovskites with enhanced performance and stability. *J. Mater. Chem. A* **2017**, *5*, 11450–11461. [[CrossRef](#)]
22. Wu, Y.; Xie, F.; Chen, H.; Yang, X.; Su, H.; Cai, M.; Zhou, Z.; Noda, T.; Han, L. Thermally stable mapbi<sub>3</sub> perovskite solar cells with efficiency of 19.19% and area over 1 cm<sup>2</sup> achieved by additive engineering. *Adv. Mater.* **2017**, *1701073*. [[CrossRef](#)] [[PubMed](#)]
23. Wang, C.L.; Zhao, D.W.; Yu, Y.; Shrestha, N.; Grice, C.R.; Liao, W.Q.; Cimaroli, A.J.; Chen, J.; Ellingson, R.J.; Zhao, X.Z.; et al. Compositional and morphological engineering of mixed cation perovskite films for highly efficient planar and flexible solar cells with reduced hysteresis. *Nano Energy* **2017**, *35*, 223–232. [[CrossRef](#)]
24. Li, L.; Chen, Y.H.; Liu, Z.H.; Chen, Q.; Wang, X.D.; Zhou, H.P. The additive coordination effect on hybrids perovskite crystallization and high-performance solar cell. *Adv. Mater.* **2016**, *28*, 9862–9868. [[CrossRef](#)] [[PubMed](#)]
25. Chueh, C.-C.; Liao, C.-Y.; Zuo, F.; Williams, S.T.; Liang, P.-W.; Jen, A.K.Y. The roles of alkyl halide additives in enhancing perovskite solar cell performance. *J. Mater. Chem. A* **2015**, *3*, 9058–9062. [[CrossRef](#)]
26. Chang, C.Y.; Chu, C.Y.; Huang, Y.C.; Huang, C.W.; Chang, S.Y.; Chen, C.A.; Chao, C.Y.; Su, W.F. Tuning perovskite morphology by polymer additive for high efficiency solar cell. *ACS Appl. Mater. Interfaces* **2015**, *7*, 4955–4961. [[CrossRef](#)] [[PubMed](#)]
27. Liang, P.W.; Liao, C.Y.; Chueh, C.C.; Zuo, F.; Williams, S.T.; Xin, X.K.; Lin, J.; Jen, A.K. Additive enhanced crystallization of solution-processed perovskite for highly efficient planar-heterojunction solar cells. *Adv. Mater.* **2014**, *26*, 3748–3754. [[CrossRef](#)] [[PubMed](#)]
28. Yantara, N.; Yanan, F.; Shi, C.; Dewi, H.A.; Boix, P.P.; Mhaisalkar, S.G.; Mathews, N. Unravelling the effects of cl addition in single step  $\text{CH}_3\text{NH}_3\text{PbI}_3$  perovskite solar cells. *Chem. Mater.* **2015**, *27*, 2309–2314. [[CrossRef](#)]
29. Dong, G.H.; Ye, T.L.; Pang, B.Y.; Yang, Y.L.; Sheng, L.; Shi, Y.; Fan, R.Q.; Wei, L.G.; Su, T. HONH<sub>3</sub>Cl optimized  $\text{CH}_3\text{NH}_3\text{PbI}_3$  films for improving performance of planar heterojunction perovskite solar cells via a one-step route. *Phys. Chem. Chem. Phys.* **2016**, *18*, 26254–26261. [[CrossRef](#)] [[PubMed](#)]

30. Bi, D.; Gao, P.; Scopelliti, R.; Oveisi, E.; Luo, J.; Gratzel, M.; Hagfeldt, A.; Nazeeruddin, M.K. High-performance perovskite solar cells with enhanced environmental stability based on amphiphile-modified  $\text{CH}_3\text{NH}_3\text{PbI}_3$ . *Adv. Mater.* **2016**, *28*, 2910–2915. [CrossRef] [PubMed]
31. Ke, W.; Xiao, C.; Wang, C.; Saparov, B.; Duan, H.-S.; Zhao, D.; Xiao, Z.; Schulz, P.; Harvey, S.P.; Liao, W.; et al. Employing lead thiocyanate additive to reduce the hysteresis and boost the fill factor of planar perovskite solar cells. *Adv. Mater.* **2016**, *28*, 5214–5221. [CrossRef] [PubMed]
32. Fei, C.; Guo, L.; Li, B.; Zhang, R.; Fu, H.; Tian, J.; Cao, G. Controlled growth of textured perovskite films towards high performance solar cells. *Nano Energy* **2016**, *27*, 17–26. [CrossRef]
33. Boopathi, K.M.; Mohan, R.; Huang, T.-Y.; Budiawan, W.; Lin, M.-Y.; Lee, C.-H.; Ho, K.-C.; Chu, C.-W. Synergistic improvements in stability and performance of lead iodide perovskite solar cells incorporating salt additives. *J. Mater. Chem. A* **2016**, *4*, 1591–1597. [CrossRef]
34. Tsai, H.; Nie, W.; Cheruku, P.; Mack, N.H.; Xu, P.; Gupta, G.; Mohite, A.D.; Wang, H.-L. Optimizing composition and morphology for large-grain perovskite solar cells via chemical control. *Chem. Mater.* **2015**, *27*, 5570–5576. [CrossRef]
35. Gong, X.; Li, M.; Shi, X.-B.; Ma, H.; Wang, Z.-K.; Liao, L.-S. Controllable perovskite crystallization by water additive for high-performance solar cells. *Adv. Funct. Mater.* **2015**, *25*, 6671–6678. [CrossRef]
36. Zhao, B.G.; Zhu, L.; Zhao, Y.L.; Yang, Y.; Song, J.; Gu, X.Q.; Xing, Z.; Qiang, Y.H. Improved performance of perovskite solar cell by controlling  $\text{CH}_3\text{NH}_3\text{PbI}_{3-x}\text{Cl}_x$  film morphology with  $\text{CH}_3\text{NH}_3\text{Cl}$ -assisted method. *J. Mater. Sci. Mater. Electron.* **2016**, *27*, 10869–10876. [CrossRef]
37. Xie, F.X.; Su, H.; Mao, J.; Wong, K.S.; Choy, W.C.H. Evolution of diffusion length and trap state induced by chloride in perovskite solar cell. *J. Phys. Chem. C* **2016**, *120*, 21248–21253. [CrossRef]
38. Bi, C.; Zheng, X.; Chen, B.; Wei, H.; Huang, J. Spontaneous passivation of hybrid perovskite by sodium ions from glass substrates: Mysterious enhancement of device efficiency revealed. *ACS Energy Lett.* **2017**, *2*, 1400–1406. [CrossRef]
39. Dar, M.I.; Abdi-Jalebi, M.; Arora, N.; Gratzel, M.; Nazeeruddin, M.K. Growth engineering of  $\text{CH}_3\text{NH}_3\text{PbI}_3$  structures for high-efficiency solar cells. *Adv. Energy Mater.* **2016**, *6*, 1501358. [CrossRef]
40. Bag, S.; Deneault, J.R.; Durstock, M.F. Aerosol-jet-assisted thin-film growth of  $\text{CH}_3\text{NH}_3\text{PbI}_3$  perovskites—a means to achieve high quality, defect-free films for efficient solar cells. *Adv. Energy Mater.* **2017**, *1701151*. [CrossRef]
41. Della Gaspera, E.; Peng, Y.; Hou, Q.; Spiccia, L.; Bach, U.; Jasieniak, J.J.; Cheng, Y.-B. Ultra-thin high efficiency semitransparent perovskite solar cells. *Nano Energy* **2015**, *13*, 249–257. [CrossRef]
42. Bag, S.; Durstock, M.F. Efficient semi-transparent planar perovskite solar cells using a ‘molecular glue’. *Nano Energy* **2016**, *30*, 542–548. [CrossRef]
43. Sveinbjörnsson, K.; Aitola, K.; Zhang, J.; Johansson, M.B.; Zhang, X.; Correa-Baena, J.-P.; Hagfeldt, A.; Boschloo, G.; Johansson, E.M.J. Ambient air-processed mixed-ion perovskites for high-efficiency solar cells. *J. Mater. Chem. A* **2016**, *4*, 16536–16545. [CrossRef]



© 2017 by the authors. Licensee MDPI, Basel, Switzerland. This article is an open access article distributed under the terms and conditions of the Creative Commons Attribution (CC BY) license (<http://creativecommons.org/licenses/by/4.0/>).